

Shear capacity of a novel joint between corrugated steel web and concrete lower slab

Wang, Sihao; He, Jun; Liu, Yuqing; Li, Chuanxi; Xin, Haohui

DOI

[10.1016/j.conbuildmat.2017.12.114](https://doi.org/10.1016/j.conbuildmat.2017.12.114)

Publication date

2018

Document Version

Submitted manuscript

Published in

Construction and Building Materials

Citation (APA)

Wang, S., He, J., Liu, Y., Li, C., & Xin, H. (2018). Shear capacity of a novel joint between corrugated steel web and concrete lower slab. *Construction and Building Materials*, 163, 360-375. <https://doi.org/10.1016/j.conbuildmat.2017.12.114>

Important note

To cite this publication, please use the final published version (if applicable). Please check the document version above.

Copyright

Other than for strictly personal use, it is not permitted to download, forward or distribute the text or part of it, without the consent of the author(s) and/or copyright holder(s), unless the work is under an open content license such as Creative Commons.

Takedown policy

Please contact us and provide details if you believe this document breaches copyrights. We will remove access to the work immediately and investigate your claim.

Shear capacity of a novel joint between corrugated steel web and concrete lower slab

Sihao Wang^a, Jun He^{b,*}, Yuqing Liu^a, Chuanxi Li^b, Haohui Xin^{a,c}

^a Department of Bridge Engineering, Tongji University, Shanghai, China

^b School of Civil Engineering, Changsha University of Science & Technology, Hunan, China

^c Department of Civil Engineering and Geosciences, Delft University of Technology, Netherland

* Corresponding author. Tel.: +86 18008466632; fax: +86 0731 85256006

E-mail address: frankhejun@163.com

Abstract

Composite girder with corrugated steel web is one of the promising concrete-steel hybrid structures with superior properties and cost effectiveness widely applied in highway and railway bridges. The connection between concrete slabs and corrugated steel web is an important part of such composite structure. In order to improve pouring quality and durability of concrete for joint structure between corrugated steel webs and concrete lower slab, the validity of placing lower slab on the inner side of corrugated steel webs was confirmed and a new joint structure with perforated plate connectors was proposed. Push-out tests on proposed joint structure with different parameters including the welding width and the plate thickness were carried out to study their shear strength, shear stiffness, failure modes and relative slip characteristics. Subsequently, three-dimensional finite element models taking material non-linearity and nonlinear contact between steel and concrete interface into consideration were built and validated by the push-out tests. Afterwards, parametric studies were performed to further investigate the influences of geometrical parameters (such as width, height and thickness of perforated steel plate) and material parameters including steel yielding strength and concrete compressive strength on ultimate shear strength and failure mode of the joint structure. Analytical results indicate that the shear loading capacity is increased with the thickness, the width and height of perforated plate, and the compressive strength of concrete. However, steel yielding strength, presence or absence of perforating rebar, have a negligible effect on ultimate shear strength of the joint structure. Finally, prediction equations of shear capacity were provided and compared with experimental and numerical results. The calculated shear capacity agrees well with experimental and numerical ones, indicating provided analytical equations can accurately predict shear capacity for such novel joint structure.

Keywords: Composite girder; corrugated steel web; joint structure; push-out tests; finite element analysis; shear capacity

1. Introduction

A composite girder with corrugated steel web, including corrugated steel webs, reinforced concrete or pre-stressed concrete slabs, is one of the promising concrete-steel hybrid structures applied to railway and highway bridges. Because of using corrugated steel webs instead of concrete webs, no restraint between the concrete slabs and corrugated steel webs exists, resulting in reduction of effects on structural responses due to shrinkage and creep of concrete, temperature differences between webs and slabs. In addition, the “accordion effect” of the corrugated steel webs allows pre-stressing efficiently introduced into concrete slabs [1, 2]. Since the first composite bridge with corrugated steel webs-Cognac Bridge built at France in 1986, a large number of this type composite bridge has been constructed, and their mechanic behaviors such as shear, flexural, torsional behavior, fatigue performance and so on have been experimentally and analytically studied [3-9].

The connection between concrete and steel is an important part of composite structure. The shear studs, Perfo-Bond Strip (PBL) connectors and angle shear connectors welded on steel flange or the corrugated steel web directly embedded in concrete slab are generally used for the joint part as shown in Fig.1. He *et al.* [10] investigated composite bridges with corrugated webs domestic and abroad to analyze the number and proportion of different kind connectors, and found that headed studs were adopted most for corrugated web bridge in early time [11-13], such as Shinkai Bridge [14] in Japan and Altwipfergrund Bridge [15] in Germany. Angel connector [16] (Fig.1 d) was the most popular one used in France and Japan, the U-shaped reinforcements welded on the angel help the connector deform ductile, while the longitudinal reinforcements bear out-of-plane bending moment.

In the eighties of last century, the PBL connector was developed for the design of the third bridge over the Caroni River in Venezuela by a German company [17]. PBL shear connectors showed better fatigue strength in comparison to welded studs from push-out test results [18]. However the out-of-plane bending moment performance for single perforated plate is not so good, therefore studs are welded on both sides of perforated plate in Fig.1 (c) or Twin PBL connectors (in Fig.1 b) are used to improve transversal bending moment resistance. Ebina *et al.* [19, 20] conducted an extensive research using normal and high performance concrete to obtain the mechanical characteristics (shear and out-plane bending behavior) of twin PBL connectors. Corrugated steel webs have very low axial rigidity, which requires relatively flexible shear connectors. A type of shear connector without using a top steel flange was proposed. Corrugated steel web embedded in the concrete as shear connector was initiated in Hondani Bridge. Nakasu *et al.* [21] carried out the experiments and finite element analysis for several types of specimens changing plate thicknesses

and embedded depths of corrugated steel webs to investigate a long-term behavior of embedded connector. Kosa *et al.* [22] conducted experimental and analytical investigations on shear and flexural behavior of composite girders with corrugated steel webs to understand failure mechanism of embedded connection. Taira *et al.* [23] investigated the stress distribution in embedded connection zone by finite element method considering the effects of embedded depth, thickness of corrugated steel plate, and the direction of wedding joint. Novák & Röhm [24], Röhm & Novák [25] investigated the load-carrying capacity of an embedded corrugated steel web with concrete dowels under longitudinal shear force and transverse bending moment respectively. Based on these studies, simplified design methods for shear connection at ultimate limit state were proposed. Kim *et.al* [26] carried out push-out test of corrugated perfo-bond rib shear connections. Test results showed that the failure was determined by concrete at inclined panel with small deformations, and shear strength increased much in comparison to standard perfo-bond rib connector due to the shear resistance of the inclined rib panel.

When stud or embedded connections used for the joints between corrugated steel webs and concrete lower slab, the designer and constructor must take care about the construction quality of concrete and waterproofing of the joints. With a view to these problems, Ono *et al.* [27] prepared some specimens of the embedded connection and carried out accelerated corrosion tests of these specimens. The results showed that durability of the embedded connection was improved by sealing the border between steel and concrete and by painting embedded connection in concrete. Shiji *et al.* [28] and He *et al.* [10] adopted the joint structures with headed studs and perforated plate connector as shown in Fig.2, the validity of placing lower slab on the inner side of corrugated steel webs was confirmed. It was proved that the bottom flange was beneficial to concrete construction quality, as well as the durability of the interface between concrete slab and corrugate web. This study only focuses on the shear behavior of joint structure with perforated plate connector.

Since shear loading capacity, failure modes and relative slip characteristics of proposed joint structures are different from those of conventional ones. Therefore, standard push-out tests are conducted to investigate the influence of different parameters (thickness of perforated plate, and width of weld seam) on the shear behavior. Then, finite element models considering both material and contact nonlinearity are built, and parametric analyses are performed to determine the influences of relative parameters on shear loading capacity. Finally, based on the results of finite element parametric analyses, calculation equations for predicting shear strength are proposed. The experimental and analytical studies may provide a reference for the design and construction of such novel joint structure in composite bridges with corrugated steel webs.

2. Experimental program

2.1 Test specimens

Referring to standard push-out test of headed stud connector [29], punching shear tests of plate

dowel [10, 28] were conducted to investigate shear capacity and relative slip. The push-out test specimens are shown in Fig.3. The width and thickness of concrete block was 500mm and 455mm, respectively. The distance from plate dowel to concrete block bottom should be large enough to prevent local damage of concrete block, which was adopted as 750mm. These push-out tests focused on shear capacity of perforated plate connectors in perpendicular direction, so the diameter of perforating rebar through 53mm-diameter holes was chosen as 13mm to meet the minimum reinforcement requirement.

Three groups of test specimens with different parameters including thickness of perforated plate, welding width between perforated plate and steel web were considered. And each group had three specimens, in which two specimens were tested under monotonous loading, and the remained one was subjected to cyclic loading. The details of all the specimen's parameters are shown in Table 1, including the concrete compressive strength, the value outside and inside the brackets represent the compressive strength of test specimen under monotonous and cyclic loading respectively. The yielding and tensile strength of steel plate for specimen SP1 and SP2 are 426MPa and 564MPa respectively, while for specimen SP3 are 433MPa and 548MPa respectively. And the yielding and tensile strength of steel reinforcements for all the specimens are 343MPa and 511MPa respectively.

2.2 Loading and measurements

Push-out test specimens were loaded in a hydraulic testing machine system. A loading plate was installed at the top in order to achieve a uniformly distributed load applied to each specimen. At the bottom of the concrete blocks, a layer of fine sand was paved to make sure the applied load evenly transfer from concrete blocks to test bench and to reduce concentrated reaction forces between specimens and the test bench. For monotonic tests of the first two specimens in each group, force control was adopted with a rate of 5kN/min till 70% of the expected failure load. Subsequently, displacement control was used until the load dropped to 80% of the maximum load or obvious failure of the specimen was observed. The loading rate for displacement control stage is 0.5 mm/min. For the third specimen under uniaxial cyclic loading, the force control was adopted in the initial loading stage. Seven loading cycles were applied with an increment of 10% of the tested average ultimate shear load of the first two specimens. After these loading cycles, monotonic load was subsequently applied until complete failure of the test specimen.

Four linear variable differential transformers (LVDTs) were symmetrically mounted at both the front and back sides of the specimen, and fixed at the same height as the middle surface of perforated plate connector, as shown in Fig. 4. The relative slip between the steel perforated plate and the concrete block was measured by averaging the output of the four gauges. The applied load and relative slips were recorded continuously and automatically. In addition, in order to investigate the stress distribution of perforated plate connector under shear load, the strains were measured along the welding position between the web and perforated plate connector in the perpendicular direction, as shown in Fig.5.

3. Finite element analysis

3.1 FE model building

The nonlinear finite element analysis (FEA) program ABAQUS [30] was used to simulate push-out tests. As shown in Fig. 6, due to symmetry property, a half of push-out test specimen with one perforated plate connector was built. The main components of the push-out specimens, including the concrete blocks, the steel plates, the bases plate, the reinforcements and perforated plate connector were simulated. Material nonlinearity and the interaction between different components were properly considered. Different mesh sizes, element types and interactions were also studied to ensure a reliable and efficiency model.

Element type greatly influences the accuracy and efficiency of the modeling. The 3-dimensional 8-node reduced integration solid element (C3D8R) was adopted to simulate the concrete block, steel plate, perforated plate connectors and perforating rebar. Other reinforcements were simulated by 3-dimensional 2-node truss elements (T3D2). The discrete rigid element (R3D4) was introduced to mesh the base plate. The global mesh was using an overall size of 15 mm, in order to reduce the computation time, however, the local mesh with small size of 5mm was refined at the area around the hole of perforated plate to give more accurate predictions of the failure mode and load-slip curve.

3.2 Interaction and boundary conditions

Symmetric boundary condition was adopted at specimen's symmetric plane, that all nodes at this surface were restricted from moving in X direction, as shown in figure 6(a). The base plate was built to simulate the test bench, and translational movement and rotation were restricted for the reference point of the base plate. The vertical displacement as shear loading was imposed at the top of loading plate, and the displacement loading was applied smoothly to reduce the impact of inertial forces. The loading rate was firstly adopted to be 1.0 mm/s and then decreased gradually to an acceptable value of 0.1 mm/s.

The separate components including steel plates and concrete blocks were assembled properly to form a half specimen model, as shown in Fig. 6(a). The perforating rebars were tied to the surrounding concrete, but the other reinforcements were embedded in concrete blocks. Perfect bond condition between reinforcements and surrounding concrete was supposed without considering the slip and de-bond of reinforcement. However, the interfaces between perforated plates and concrete blocks in normal and tangential direction were simulated by hard contact and frictional formulation, respectively. The friction coefficient is chosen as 0.6 in the contact boundary between base plate and concrete blocks, while the friction coefficient for interactions between concrete blocks and steel plates was assumed to be 0.4.

3.3 Material modeling

3.3.1 Concrete properties

For the simulations of joint structure in push-out test, the nonlinear behavior of concrete was presented by a uniaxial compressive and a tensile stress-strain curve in compression and tension respectively, as shown in Fig.7.

The stress (σ_c) vs. strain (ε_c) curve of concrete in compression is divided into two parts. The first part (Eq. 1) is assumed to be ascending stage when the stress is less than concrete compressive strength, f_c .

$$\sigma_{c1} = \frac{nf_c \varepsilon_c}{n-1 + (\varepsilon / \varepsilon_p)^n} \quad (1)$$

where, $n = E_c \varepsilon_{cp} / (E_c \varepsilon_{cp} - f_{cp})$, and E_c is the Young's modulus (MPa), ε_{cp} is the strain corresponding to compressive strength f_c .

The second part (Eq. 2) of the strain-stress curve is a descending stage, and the ultimate compressive strain ε_{cu} is defined as the strain related to corresponding stress decreased to $0.5 f_c$.

$$\sigma_{c2} = \frac{f_c \varepsilon_c / \varepsilon_{cp}}{\alpha_c (\varepsilon_c / \varepsilon_{cp} - 1)^2 + \varepsilon_c / \varepsilon_{cp}} \quad (2)$$

where α_c is a parameter at descending stage of compressive stress-strain curve which can be determined according to f_c recommended in GB50010 [31].

The stress (σ_t) vs. strain (ε_t) curve of concrete in tension also includes two parts. Equation 3 is suggested to represent the ascending branch of concrete in tension.

$$\sigma_{t1} = [1.2(\varepsilon_t / \varepsilon_{tp}) - 0.2(\varepsilon_t / \varepsilon_{tp})^6] f_t \quad (3)$$

where ε_{tp} is the tensile strain corresponding to ultimate tensile strength f_t .

The descending section of the tensile stress-strain curve from ε_{tp} to the ultimate tensile strain ε_{tu} is described by Eq. 4.

$$\sigma_{t2} = \frac{f_t \varepsilon_t / \varepsilon_{tp}}{\alpha_t (\varepsilon_t / \varepsilon_{tp} - 1)^{1.7} + \varepsilon_t / \varepsilon_{tp}} \quad (4)$$

where α_t is a parameter at descending stage of tensile stress-strain curve which can be determined according to f_t referred in GB50010; ε_{tu} is ultimate tensile strain, assumed to be $10\varepsilon_{tp}$.

The concrete-damage plasticity model was adopted to describe the degraded response of concrete, five important plasticity parameters were provided in simulation. The dilation angle ψ , according to reference [32], was selected as an intermediate value, $\psi=30^\circ$. As recommended by ABAQUS user manual, the other parameters such as flow potential eccentricity $\varepsilon=0.1$, viscosity parameter $\mu=0$, the biaxial to uniaxial compressive strength ratio $\sigma_{b0}/\sigma_{c0}=1.16$, and the ratio of second stress invariant on the tensile meridian to that on the compressive meridian $K = 2/3$.

3.3.2 Steel properties

The relation of stress vs. strain for steel plates and steel reinforcements was represented by the tri-linear curve with strain hardening, as shown in Fig.8, in which f_y , f_u , ϵ_y and ϵ_u are yield stress, ultimate strength, yield strain and ultimate strain, respectively. The stress increases linearly with strain in initial elastic stage, and afterward into the stage of yielding, finally followed by a strain hardening branch. The stress-strain relationships of steel in compression part are assumed the same as that in tension part. Based on material test, the Young's modulus E_s is 206GPa and the ultimate strain ϵ_u is set as 20% for steel plates, while E_s and ϵ_u are taken as 200GPa and 7.5% for steel reinforcements.

4. Experimental and FE analytical results

4.1 Failure modes

All the specimens are failure due to the concrete crush at the position of perforated plate connector including specimen SP2 whose idea failure place expected to weld part. The concrete punching shear failure was occurred on the corner of shear connector for all specimens in push-out tests, as shown in Fig.9 (a), also the maximum strains of concrete block from FEA (Fig.9b) appeared at the same position as that from push out test under ultimate state. The initial crack occurred at concrete block below perforated plate. With increasing applied shear load, cracks gradually developed toward the bottom of concrete block, mostly in the neighborhood of shear connector.

After push-out tests, the specimens under cyclic loading were dismantled and concrete blocks were cut off directly at the place of perforated plate to investigate the inner failure condition, Fig.10 (a) shows the inside concrete crack pattern, in addition, the shape of perforated plate was marked on the concrete block for comparison, Fig.10 (b) represents simulated strains of concrete block below the perforated plate at the ultimate state. It was found that the effective zone of compressive concrete is approximate in triangle shape.

Concrete in the disassembly specimen was removed to observe the deformation of perforated plate. The plate deformation at free end without welding was found in specimen SP1 and SP2 due to local yielding of perforated plate at fixed end with welding, as shown in Fig. 11, in which the FEA result represents the deformation of the perforated plate at the ultimate state. As for the deformation of perforated plate, specimen SP2 was the largest, while specimen SP3 was almost intact after loading.

The failure modes observed from the FE analysis were almost coincided to that from push-out tests, as shown in Figs. 9-11. The local deformation of perforated plate simulated by FE model (Fig.11b) occurred at the same place with almost some magnitude, in comparison to that from test results. Also the initiation and development of concrete cracks, the inside crack pattern at failure can be simulated by finite element analysis.

4.2 Load-slip relation

The relative slip at steel-concrete interface between concrete block and steel plate initiated and developed with the applied load. The relation between relative slip and shear load for specimens under monotonous loading (SP-1,2) and cyclic loading (SP-3) is plotted in Fig. 12, where the load-slip curve for specimens under cyclic loading is the envelope curve and the residual slip is obtained after unloading for each load cycle. The load-slip relationship is nearly linear up to 1/3 of the maximum load, therefore, the shear stiffness, k_s , is defined as the secant modulus at the point of load-slip curve where load is applied to 1/3 maximum load. The simulated load-slip curves under monotonous loading from finite element analysis agree well with experimental results in terms of both ultimate shear strength and shear stiffness. Moreover, the peak slip corresponding to ultimate shear strength from FE simulation under monotonous loading is almost the same as that from push-out test.

The shear strength (V_u), shear stiffness (k_s) and peak slip (s_p) for specimens under monotonous loading from finite element analysis (FEA) are summarized in Tables 2 and are compared with the mean values of the test results. The shear strength (V_u) is defined as the maximum load during the tests. The shear stiffness (k_s) represents the secant slope at 1/3 of the maximum load, as mentioned before. The shear stiffness which reflects deformation capacity of perforated plate connector changed from 1000 to 3000kN/mm for all specimens. The slip deformation is evaluated by the peak slip (s_p), which is the slip corresponding to shear strength. The peak slip for specimen SP2 was the largest of all specimens, and the perforated plate connector showed plastic behavior. However, the peak slip for specimens SP3 was relatively small, and the perforated plate connector showed brittle behavior. In addition, the difference between slip under monotonous and slip under cyclic load is inclined to become large as increasing load. In regard to the residual slip, the value changed obviously for specimen SP2 under the ultimate shear force, but changed slightly for specimen SP1, and almost kept invariant for specimen SP3, the residual slip under ultimate shear force is 0.52mm, 0.86mm and 0.14mm for specimens SP1, 2, and 3 respectively. As a primary factor, the perforated plate deformation due to local yield near welding part affects the residual slip performance.

In comparison of FE analytical results to push-out test ones, the mean values of $V_{u,FEA}/V_{u,test}$, $k_{e,FEA}/k_{e,test}$ and $s_{p,FEA}/s_{p,test}$ ratios are 0.98, 0.82 and 1.30, respectively, with the corresponding coefficients of variations of 0.09, 0.14 and 0.28, respectively. Therefore, the proposed finite element model can reasonably predict the shear behavior of perforated plate connector and thus is reliable for the following parametric study.

4.3 Strain results

Figure 13 shows the strain on perforated plate of each specimen at initial elastic stage ($V_u/3$) under monotonous loading, and tensile strain is defined as positive. The position and label of strain

gauges on the plate are shown in Fig.5. It can be found that the strain magnitude was large at the end of the welding leg between perforated plate and the web or flange. Tensile strain of specimen SP2 with small welding leg was larger than that of specimen SP1, since the perforated plate deformed easily with short welding leg. In comparison with specimen SP1, both tensile and compressive strains were smaller for specimen SP3 with long welding leg and thick plate, the main reason is that perforated plate deformation is restrained as the increase of the welding length and plate thickness, as well the concrete compressive stress. In addition, the strain magnitude and distribution from FE analysis agree well with that from measurements for all the specimens, except the strain near corner (S3 and L5) for specimen SP1. The simulated strain near corner is in tension and the value is very small, however the measured strain at this position is in compression with relative small value, which results in the some deviation between tested and simulated strain for S3 and L5 for specimen SP1. The comparison of strain results indicate that finite element model can predict the magnitude and distribution of stain on perforated plate within sufficient accuracy.

5. Parametric study

Using the verified finite element model, a series of push out tests was simulated to study the influences of geometrical parameters (such as width- b , height- h and thickness- t of steel perforated plate, as shown in Fig.3) and material parameters including the steel yielding strength and concrete compressive strength on shear capacity of joint structure. On the basis of test specimen SP1, only some parameters (bold entries in the table) of simulated models are varied, all these models are listed in Table 3. The constitutive models of materials, the boundary conditions and the interaction are set the same as the verified FE model.

5.1 Effect of perforated plate width

In order to examine the effect of perforated plate width on ultimate shear strength, the width at $b=140\text{mm}$, 160mm , 180mm and 200mm was selected in the FE models. Figure 14 shows the load-slip curves and illustrates the effect of perforated plate width on shear loading capacity. It can be found that the ultimate shear strength increased linearly with the increasing of perforated plate width, and the perforated plate width slightly affect the initial shear stiffness at elastic stage, but the increase of width can improve both shear strength and shear stiffness at ultimate state obviously.

5.2 Effect of perforated plate height

The height of perforated plate at $h=300\text{ mm}$, 350 mm , 400 mm and 450 mm was chosen in simulated models based on specimen SP1. Figure 15 shows the effect of perforated plate height on ultimate shear strength, the increase of perforated plate height improves both shear strength and shear stiffness of perforated plate connector, and ultimate shear strength is in linear proportion to

perforated plate height.

5.3 Effect of perforated plate thickness

The thickness of perforated plate was taken as $t=10$ mm, 12 mm, 14 mm and 16 mm to consider their effect on shear behavior. Figure 16 shows the effect of perforated plate thickness on ultimate shear strength. The shear loading capacity increases linearly as the increase of plate thickness. In addition, the increase of perforated plate thickness enhance not only the shear strength but also shear stiffness, however, shear stiffness increase more obvious as the thickness from 10mm to 12mm than that from 14mm to 16mm.

5.4 Effect of steel yield strength

The yielding strength of steel perforated plate was selected as $f_y=345$ MPa, 420MPa, 500MPa and 550MPa (Table. 3) to investigate their influence on shear loading capacity. The load-slip curves, the relation between shear loading and steel yield strength are shown in Fig. 17, the shear capacity increased slightly as the increase of steel yield strength, only 10% of shear strength is improved as steel yield strength increasing from 345MPa to 550MPa. In addition, the steel yield strength has little influence on the shear stiffness of perforated plate connector.

5.5 Effect of concrete compressive strength

The compressive strength of concrete block was taken as $f_c=32$ MPa, 37.8MPa, 46MPa and 52.5MPa (Table. 3) to study their effect on shear loading capacity. The load-slip curves, the relation between shear loading and concrete compressive strength are shown in Fig. 18, the ultimate shear strength increased nonlinearly with concrete compressive strength. Moreover, the shear strength increases obviously when using normal concrete with low compressive strength, but increase slowly when using high strength concrete, since the increase of concrete strength may change specimen failure from concrete crush to steel plate yielding. In addition, concrete compressive strength has slight effect on initial shear stiffness at elastic stage, but obvious influence on shear stiffness at ultimate state.

5.6 Effect of perforating rebar

In order to investigate the effect of presence or absence of perforating rebar on shear loading capacity, three specimens were considered: specimen with perforating rebar, specimen without perforating rebar, and specimen without both hole and rebar, as shown in Table 3. The load-slip curves, the relation between shear load and steel perforating rebar are shown in Fig. 19. In

comparison to specimen SP1, shear strength is reduced only by 6% and 7% for specimen without perforating rebar and specimen without both hole and rebar, respectively. Moreover, perforating rebar has no effect on shear stiffness till ultimate state. Therefore, arrangement of perforating rebar is needed only to meet the minimum reinforcement requirements.

6. Simplified calculation

6.1 Shear strength

From the experimental and numerical results of failure mode and stress distribution on perforated plate connectors in push-out test, it can be found that the structural behavior and load transmission mechanism of proposed shear connectors are similar to that of channel and angel shear connectors. Therefore, the ultimate load capacity of proposed shear connector is estimated and evaluated by the calculation formulas which have been developed for the channel and angel shear connectors.

On the basis of push-out test results of channel shear connectors conducted by Viest *et al.* [33], Slutter & Driscoll [34] proposed an empirical equation to estimate the ultimate strength of channel shear connectors, which was later modified and presented in the American Institute of Steel Construction specification [35] in the following:

$$V_n = 0.3(t_f + 0.5t_w)L_c\sqrt{f'_c E_c} \quad (5)$$

where V_n is nominal shear strength of a channel shear connector embedded in a solid concrete slab (N); t_f and t_w are the thickness of flange and web of channel shear connector respectively (mm); L_c is the length of channel shear connector (mm); f'_c is compressive strength of concrete (MPa); E_c is Young's modulus of concrete (MPa).

The Canadian standard CAN/CSA-S16-01 [36] also provides a similar equation which can be implemented for calculating the shear capacity of a channel shear connector:

$$V_n = 36.5(t_f + 0.5t_w)L_c\sqrt{f'_c} \quad (6)$$

The meaning of parameters in Eq.(6) is the same as that in Eq.(5).

As for the angle or block type shear connectors, Eurocode 4 [37] suggests the following equation for calculating the loading capacity:

$$V_n = \eta A_{f1} f_{ck} / \gamma_c \quad (7)$$

where: η is equal to $\sqrt{A_{f2} / A_{f1}}$ for block shear connector with high stiffness; A_{f1} is the area of the front bearing area of the connector; A_{f2} is the area of the front bearing area of the connector amplified at an inclination rate of 1:5 from the previous connector considering only the area inside the concrete; η is equal to 1 for angle type flexible connector; γ_c is the concrete safety factor equal to 1.5.

Also, empirical equations were developed by Ros [38] that predict the load-carrying capacity of

angle shear connectors based on either the connector failure or concrete crush:

$$V_n = \left(63 \frac{t_w}{h} + 1.60 \right) L_c h \sqrt{f'_c} \quad (8)$$

where: t_w is the thickness of shear connector (mm); h is the height of shear connector (mm); L_c is the length of connector (mm); f'_c is compressive strength of concrete (MPa).

Table 4 summarized the calculation results on shear capacity of push-out test specimens by the equations (5)~(8), also these predicted shear capacity were compared to tested ones in order to evaluate the applicability of those calculation equations. Since the perforated plate connectors do not have flange at top, the value of t_f in equations (5, 6) is taken as zero. It can be found that the equations (5, 6) implemented for calculating the shear capacity of a channel shear connector suggested by AISC specification and CAN/CSA-S16-01 underestimate the shear capacity of novel perforated plate connectors, the mean values of $V_{eq,5}/V_{u_test}$ and $V_{eq,6}/V_{u_test}$ are 0.67 and 0.45, respectively. And the equation (8) provided to predict load-carrying capacity of angle shear connectors overestimate the shear capacity of perforated plate connectors too much, since the mean values of $V_{eq,8}/V_{u_test}$ is 2.04. In comparison of calculated shear capacity to test results, equation (7) suggested by Eurocode 4 [37] is the most suitable one among the above mentioned equations to predict shear capacity of perforated plate connectors, the average value of the ratio of $V_{eq,8}/V_{u_test}$ is 1.25. Therefore, equation (7) will be modified to estimate shear capacity of perforated plate connectors more accurately considering their structural characteristics.

The calculation of shear strength is then proposed referring to the calculation method of angle shear connector [37, 39] with the similar resistant mechanism, which includes the compressive strength of concrete and the shearing strength of welding part. The perforated plate connector, steel web and bottom flange were welded in double sides, and the compressive area of concrete was effective in triangle-shaped area around the welding line, which was verified by experimental and FE analytical failure mode as shown in Fig.10, the shear capacity of joint structure is calculated as follows:

$$V_u = \min(R_1, R_2, R_3) \quad (9)$$

$$R_1 = A f'_{ck} / k ;$$

$$R_2 = \sum a L_1 f_y / \sqrt{3} ;$$

$$R_3 = t (b + h) f_y / \sqrt{3}$$

where R_1 is compressive resistance of concrete; R_2 is shear resistance of welding part; R_3 is shear resistance of steel plate; A is effective area of plate ($A = 1/2 \cdot b \cdot h$), that is different to A_f in Eq.(7); f'_{ck} is designed standard strength of concrete; b, h, t is the width, height and thickness of perforated plate respectively; k is the reduction coefficient (1.5 for angle shear connector); a is theoretical thickness of welding; L_1 is effective length of welding; f_y is yielding strength of steel.

6.2 Comparison and discussion

Table 5 shows the calculated shear strength of push-out test specimens by Eq.(9), also the ratios of calculated values to tested ones, FEA results to test ones, FEA results to calculated ones. All the specimens are failure due to concrete crush at the position of perforated plate connector including specimen SP2 whose design failure place was welding part. So the ratio of test value to compressive resistance of concrete (R_1) for specimen SP2 is presented in the table, see the value in bracket. From the comparison in Table 5, one can found that:

(1) The shear strength could not be calculated by the shear resistance of welding if the welding length is smaller than the required value for specimen SP2 [40].

(2) The ratio of tested shear strength to calculation one for specimen SP1 has the same degree comparing with specimen SP3, indicating that the increase of plate thickness slightly affected shear strength, if perforated plate is thick enough.

Moreover, the mean values of $V_{u_test} / V_{u_Cal.}$ and $V_{u_FEA} / V_{u_Cal.}$ are 1.11 and 1.08, respectively, and the corresponding coefficients of variations are 0.14, and 0.03, respectively. Therefore, the proposed calculation equation (9) can reasonably predict shear strength of perforated plate connector with high accuracy.

In order to further verify the accuracy of shear strength calculation formula for perforated plate connector, on the basis of push-out test in present study, parametric analysis using verified finite element model was conducted in section 5, which including the geometric parameters of the perforated plate and the material parameters of joint structure, for example: the concrete compressive strength and yielding strength of perforated steel plate. The shear strength from parametric analysis results are compared with calculation ones, as shown in Fig. 20, in which the comparison of tested and calculated results is also included. The average value of the ratio of shear strength from FEA and test to theoretical calculation one is 1.01, with the corresponding coefficients of variations of 0.12, indicating that the shear strength of such joint structure can be predicted according to simplified calculation formula (9).

The reduction coefficient k in Eq. (9) was deduced by tested and FEA results to guide the design of shear strength for such joint structure. The value of k is obtained as 1.28 considering 2 times standard deviation as the upper and lower bounds, as shown in Fig.20, specimen SP2 was not included in the figure since the failure mode is different from the pre-designed one. For the safe side, k is set as 1.28 in Eq. (9) to design shear strength of perforated plate connector.

7. Concluding remark

(1) Push out tests of perforate plate connector were carried out, typical failure mode under punching shear load was observed, and the effects of key parameters including material properties, thickness of the perforated plate, width of weld seam on shear capacity and stress distribution were

clarified.

(2) Considering ideal elastic-plasticity of steel, concrete damaged plasticity model and nonlinear contact between steel and concrete interface, an efficient finite element numerical simulation method for perforated plate connector in joint structure was established and verified by test results. The failure modes and load-slip curves predicted by FE analysis agree well with that obtained from experiment.

(3) According to parametric analytical results, the width and height of perforated plate, concrete compressive strength has a significant effect on the shear loading capacity. However, the steel yield strength, presence or absence of perforating rebar, have a negligible effect on shear strength of plate dowel.

(4) Concrete damage took place in triangle form adjacent welding edge under failure loading. Shear strength calculation according to the assumption that effective compressive area of concrete accounts a half of perforated plate in triangle shape is reasonable. Based on this hypothesis, the theoretical formula of shear capacity was proposed. The theoretical analysis results are in good agreement with the experimental and FE analysis results. Also reduction coefficient k is obtained as 1.28 from test and parametrical analysis results for safe side.

All the results can provide a reference for the design of joint structure between corrugated steel web and lower concrete slab. Since this study ignores the contribution of corrugated steel web itself to shear capacity, the magnitude of its influence needs to be further studied.

Acknowledgments

This research is sponsored by National Nature Science Foundation of China (51308070, 51408070, 51378080); National Basic Research Program of China (973 Program, No. 2015CB057705); Key Discipline Fund of Creative Project of Bridge and Tunnel Engineering (13ZDXK04) from Changsha Univ. of Science and Technology, Open Fund of Hunan Province University Key Laboratory of Bridge Engineering (13KA04); and The Applied Basic Research Program of Shanxi Province. These supports are gratefully acknowledged.

Reference

- [1] He, J., Liu, Y., Chen, A., and Yoda, T. Mechanical behavior and analysis of composite bridges with corrugated steel webs: State-of-the-art. *International Journal of Steel Structures*, 2012, 12(3): 321-338.
- [2] Jiang, R., Au F.T.K, and Xiao Y. Prestressed Concrete Girder Bridges with Corrugated Steel Webs: Review. *Journal of Structural Engineering, ASCE*. 2015, 141(2): 04014108, 1-9.
- [3] Sause, R., and Braxtan, T. N. Shear strength of trapezoidal corrugated steel webs. *Journal of Constructional Steel Research*, 2011, 67: 223-236.
- [4] Mo, Y. L., and Fan, Y. Torsional design of hybrid concrete box girders. *Journal of Bridge Engineering, ASCE*, 2006, 11(3): 329-339.

- [5] Ibrahim, S. A., El-Dakhkhni, W. W., and Elgaaly, M. Fatigue of corrugated-web plate girders: Experimental study. *Journal of Structural Engineering, ASCE*, 2006, 132(9): 1371-1380.
- [6] He, J., Liu, Y., Chen, A., and Yoda, T. Shear behavior of partially encased composite I-girder with corrugated steel web: Experimental study. *Journal of Constructional Steel Research*, 2012, 77: 193-209.
- [7] He, J., Liu, Y., Lin, Z., Chen, A., and Yoda, T. Shear behavior of partially encased composite I-girder with corrugated steel web: Numerical study. *Journal of Constructional Steel Research*, 2012, 79: 166-182.
- [8] He, J., Liu, Y., Chen, A. Wang, D. and Yoda, T. Bending behavior of partially encased composite I-girder with corrugated steel web. *Thin-walled Structures*, 2014, 74: 70–84.
- [9] He, J., Liu, Y., Xu, X. and Li, L. Loading capacity evaluation of composite box girder with corrugated webs and steel tube slab. *Structural Engineering and Mechanics*, 2014, 50(4): 501-524.
- [10] He, J, Yoda, T., Shiji, A., Ohyama, H., Liu, Y. and Chen A. Joint structures of composite bridge with corrugated steel webs. *Proceeding of National Doctoral Forum in civil engineering*, Central South University, China, 2009,1-9.
- [11] Xue, D., Liu, Y., Yu, Z. and He, J. Static behavior of multi-stud shear connectors for steel-concrete composite bridge. *Journal of Constructional Steel Research*, 2012, (74):1-7.
- [12] Lin, Z. Liu, Y. and He, J. Behavior of stud connectors under combined shear and tension loads. *Engineering Structures*, 2014, (81): 362-376.
- [13] Xu, X., Liu, Y. and He, J. Study on mechanical behavior of rubber-sleeved studs for composite structure. *Construction & Building Materials*, 2014, (53): 533-546.
- [14] Kondo, M., Shimizu, Y., Kobayashi, K., and Hattori, M. Design and construction of the Shinkai Bridge-Prestressed concrete bridge using corrugated steel webs. *Bridge Found. Eng.*, 1994, 13-20.
- [15] Novák, B., Denzer, G., and Reichert, F. Validation of the structural behaviour of the Altwipfergrund Bridge. *Bautechnik*, 2007, 84: 289-300.
- [16] Shariati, M., Sulong, N.H. R., Suhatrik, M., Shariati, A., Khanouki, M.M.A., Sinaei, H. Comparison of behaviour between channel and angle shear connectors under monotonic and fully reversed cyclic loading. *Construction and Building Materials*, 2013, 38: 582-593
- [17] Leonhardt, F., Andrae, W., and Andrae, H.P. New, improved bonding means for composite load bearing structure with high fatigue strength. *Beton-und Stahlbetonbau*, 1987, 82(12):325-331.
- [18] Hosaka, T., Mitsugi, K., Hiragi, H. and Ushijima, H. Study on shear strength and design method of perfobond strip. *Journal of Structural Engineering A. JSCE*, 2002, 48(3): 1265-1272.
- [19] Ebina, T., Kutsuna, Y., Wada, T., Tategami, H., and Sonoda, K. Study on shear strength of corrugated steel web with flask shape-perfobond strip connections. *5th Symposium of hybrid structure*, Japan, 2003, 245-250.
- [20] Ebina, T., Higashida, N., Nakamura, H., Tategami, H., and Sonoda, K. Study on out-plane bending behavior of corrugated steel web with twin- perfobond strip connections. *Journal of Structural Engineering, JSCE*, 2004, 50A: 1191-1202.
- [21] Nakasu, K., Yoda, T., and Sato, K. Study on out-of-plane bending of concrete dowels in a composite girder with corrugated steel web. *Proceeding of JSCE*, 2000, 647(I-51): 267-279.
- [22] Kosa, K., Awane, S., Uchino, H., and Fujibayashi, K. Ultimate behavior of prestressed concrete bridge with corrugated steel webs using embedded connection. *Proceeding of JSCE*, 2006, 62(1): 202-220.
- [23] Taira, Y., Aoki, K., Hagiwara, N., Ito, A., and Hirose, T. Connection joint between lower slab and corrugated steel

- webs applied to PC-box girder. *Journal of Structural Engineering, JSCE*, 2009, 55A: 1066-1074.
- [24] Novák, B., and Röhm, J. The use of corrugated steel webs in bridge constructions -Load bearing behaviour of concrete dowels in combination with corrugated steel webs under longitudinal shear. *Beton- und Stahlbetonbau*, 2009, 104(9): 562-569.
- [25] Röhm, J., and Novák, B. Behavior of composite structures with corrugated steel webs under transverse bending using concrete dowels. *Beton- und Stahlbetonbau*, 2010, 105(3): 176-185.
- [26] Kim, S., Ahn, J., Choi, K., and Jung, C. Experimental evaluation of the shear resistance of corrugated perfobond rib shear connections. *Advances in Structural Engineering*, 2011, 14(2): 249-263.
- [27] Ono, K., Osada, K., Sakurada, M., and Ohura, T. Corrosion characteristics of embedded connection for prestressed concrete bridges with corrugated steel webs. *6th Symposium of hybrid structure*, Japan, 2006, 29(1-6).
- [28] Shiji, A., Ooyama, H., and Yoda, T. Experimental Study on the New Joint Structures of a Bridge with Corrugated Steel Webs. *Journal of structural engineering, JSCE*, 2008, 54A: 759-768.
- [29] Japanese steel structural society (JSSS). Push out test method and research state of art of stud connector. 1991.
- [30] ABAQUS. *Analysis User's Manual*; (version 6.10), Hibbitt, Karlsson & Sorensen, USA. 2010.
- [31] Code for design of concrete structures (GB50010), China Architecture & Building Press, China. 2010.
- [32] Pavlović, M., Marković, Z., Veljković, M., Buđevac, D. Bolted shear connectors vs. headed studs behaviour in push-out tests. *Journal of Constructional Steel Research*, 2013, 88: 134-149.
- [33] Viest IM, Siess CP, Appleton JH, Newmark NM. Full-scale tests of channel shear connectors and composite T-beams. *Univ Ill Bull* 1952:405.
- [34] Slutter RG, Driscoll GC. Flexural strength of steel-concrete composite beams. *ASCE J Struct Div* 1965;91(ST2):71-99.
- [35] AISC. Specification for structural steel buildings. Chicago (IL): AISC-360-05, American Institute of Steel Construction; 2005.
- [36] CSA. Limit states design of steel structures. CSA Standard CAN/CSA S16-01. Toronto, Ont: Canadian Standards Association (CSA); 2001.
- [37] EUROCODE 4. ENV 1994. Design of composite steel and concrete structures Part 1.1 General rules and rules for buildings. Brussels: CEN European Committee for Standardisation; 2005.
- [38] Ros S. Formulation for shear force-relative displacement relationship of L-shape shear connector in steel-concrete composite structures. PhD thesis. Japan: Kochi University of Technology Academic Resource Repository; 2011.
- [39] Pre-stressed concrete technological society (PCTS). Composite bridge design and construction standard. 2005.
- [40] Japanese highway and bridge association (JHBA). Specifications for highway bridges and explanation III: Concrete bridge. 2002.

List of Tables

Table 1 Experimental parameters

Table 2 Peak slip and shear stiffness

Table 3 Simulated models for push-out test specimens

Table 4 Comparison of shear strength

Table 5 Comparison of shear strength from test, FEA and calculation

Tables

Table 1 Experimental parameters

Specimen	Concrete		Plate connector			Yield strength /MPa	Tensile strength /MPa	Welding width	Designed failure mode
	H/mm	Compressive strength/MPa	h/mm	b/mm	t/mm			S/mm	
SP1	455	37.8(38.3)	350	160	12	426	564	9	Concrete crush
SP2	455	42.2(44.5)	350	160	12	426	564	5	Welding failure
SP3	455	36.8(38.6)	350	160	16	433	548	12	Concrete crush

Table 2 Peak slip and shear stiffness

Specimen	Loading type	Shear strength (V_u / kN)		Peak slip (s_p / mm)		Shear stiffness (kN/mm)		
		Test	FEA	Test	FEA	Test	FEA	
SP1	1,2	Monotonic	1049, 1105	1110	0.96, 1.79	1.71	1451, 1514	1424
	3	Cyclic	1072	-	1.81	-	1067	-
SP2	1,2	Monotonic	1294, 1302	1291	2.03, 1.80	2.55	3078, 2972	1945
	3	Cyclic	1298	-	4.02	-	2104	-
SP3	1,2	Monotonic	1424, 1123	1161	0.98, 0.69	0.98	2696, 2454	2223
	3	Cyclic	1062	-	1.50	-	1317	-

Table 3 Simulated models for push-out test specimens

Specimens	h/mm	b/mm	t/mm	H/mm	f_y /MPa	f_c /MPa	Perforating rebar	V_{u_FEA}	$V_{u_Cal.}$
SP1	350	160	12	455	423	37.8	yes	1110	1058
SP1-h-300	300	160	12	405	423	37.8	yes	981	907
SP1-h-400	400	160	12	505	423	37.8	yes	1211	1210
SP1-h-450	450	160	12	555	423	37.8	yes	1354	1361
SP1-b-140	350	140	12	455	423	37.8	yes	1053	926
SP1-b-180	350	180	12	455	423	37.8	yes	1150	1191
SP1-b-200	350	200	12	455	423	37.8	yes	1199	1323
SP1-t-10	350	160	10	455	423	37.8	yes	990	1058
SP1-t-14	350	160	14	455	423	37.8	yes	1199	1058
SP1-t-16	350	160	16	455	423	37.8	yes	1296	1058
SP1-fy-345	350	160	12	455	345	37.8	yes	1042	1058
SP1-fy-500	350	160	12	455	500	37.8	yes	1106	1058
SP1-fy-550	350	160	12	455	550	37.8	yes	1140	1058
SP1-fc-32	350	160	12	455	423	32	yes	920	896
SP1-fc-46	350	160	12	455	423	46	yes	1237	1288
SP1-fc-52.5	350	160	12	455	423	52.5	yes	1275	1470

SP1-nobar	350	160	12	455	423	37.8	No rebar	1045	1058
SP1-nohole	350	160	12	455	423	37.8	No hole	1034	1058

Table 4 Comparison of calculated shear strength

Specimens	Test/kN	Calculation / kN				Ratio				
	$V_{u_test.}$	$V_{Eq. 5}$	$V_{Eq. 6}$	$V_{Eq. 7}$	$V_{Eq. 8}$	$V_{Eq. 5}/V_{u_test.}$	$V_{Eq. 6}/V_{u_test.}$	$V_{Eq. 7}/V_{u_test.}$	$V_{Eq. 8}/V_{u_test.}$	
SP1	1	1049	694	471	1411	2177	0.66	0.45	1.35	2.08
	2	1105	694	471	1411	2177	0.63	0.43	1.28	1.97
	3	1072	699	474	1430	2192	0.65	0.44	1.33	2.04
SP2	1	1294	743	498	1575	2301	0.57	0.38	1.22	1.78
	2	1302	743	498	1575	2301	0.57	0.38	1.21	1.77
	3	1298	768	511	1661	2363	0.59	0.39	1.28	1.82
SP3	1	1424	910	620	1374	2684	0.64	0.44	0.96	1.88
	2	1123	910	620	1374	2684	0.81	0.55	1.22	2.39
	3	1062	937	635	1441	2748	0.88	0.60	1.36	2.59

Table 5 Comparison of shear strength from test, FEA and calculation

Specimens	Calculation / kN				Test/ kN	FEA/kN	Ratio			
	R1	R2	R3	$V_{u_Cal.}$	$V_{u_test.}$	V_{u_FEA}	$V_{u_test}/V_{u_Cal.}$	$V_{u_FEA}/V_{u_Cal.}$	V_{u_FEA}/V_{u_test}	
SP1	1	1058	1148	1299	1058	1049	1110	0.99	1.05	1.06
	2	1058	1148	1299	1058	1105	1110	1.04	1.05	1.00
	3	1072	1148	1299	1072	1072	-	0.93	-	-
SP2	1	1182	638	1299	638	1294	1291	2.03(1.1)*	1.09	1.00
	2	1182	638	1299	638	1302	1291	2.04(1.1)*	1.09	0.99
	3	1246	638	1299	638	1298	-	2.04(1.04)*	-	-
SP3	1	1030	1530	1760	1030	1424	1161	1.38	1.13	0.82
	2	1030	1530	1760	1030	1123	1161	1.09	1.13	1.03
	3	1081	1530	1760	1081	1062	-	0.98	-	-

List of Figures

Fig.1 Conventional joint structure of composite bridge with corrugated steel web

Fig.2 Joint structure between lower slab and corrugated web

Fig.3 Test specimens /mm

Fig.4 Relative slip measurement /mm

Fig.5 Strain measurement on perforated plate /mm

Fig.6 Finite element model of push-out test

Fig.7 Material constitution of concrete

Fig.8 Constitutive law for structural and reinforcement steel

Fig.9 Typical failure mode (SP3)

Fig.10 Destructive characteristics on the cutting surface (SP1)

Fig.11 Perforated plate deformation (SP2)

Fig.12 Load-slip curves

Fig.13 Strain distribution on perforated plate

Fig.14 Effect of perforated plate width

Fig.15 Effect of perforated plate height

Fig.16 Effect of perforated plate thickness

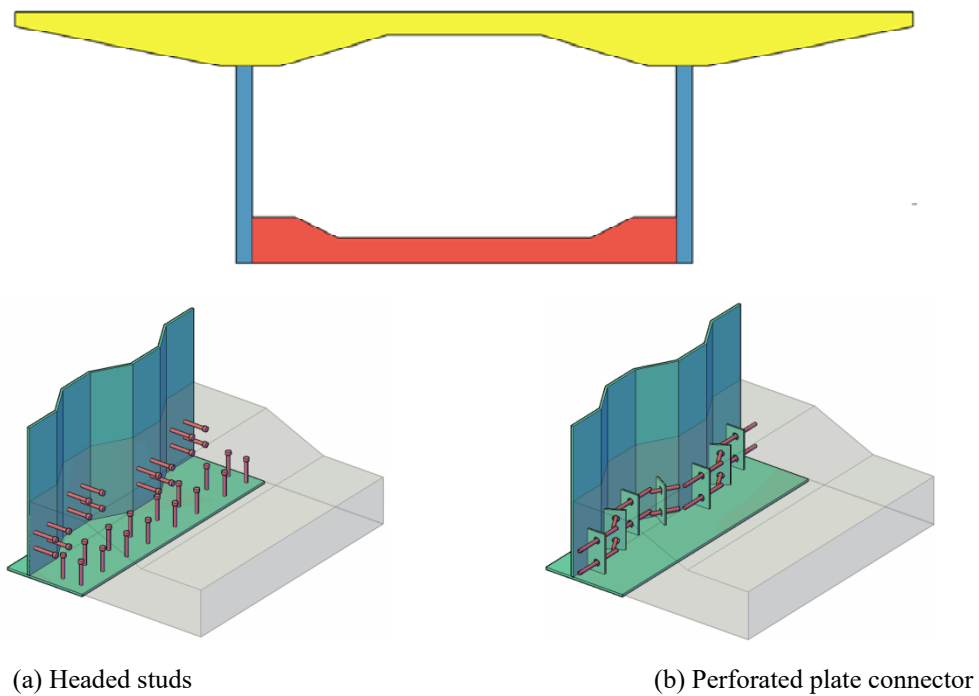
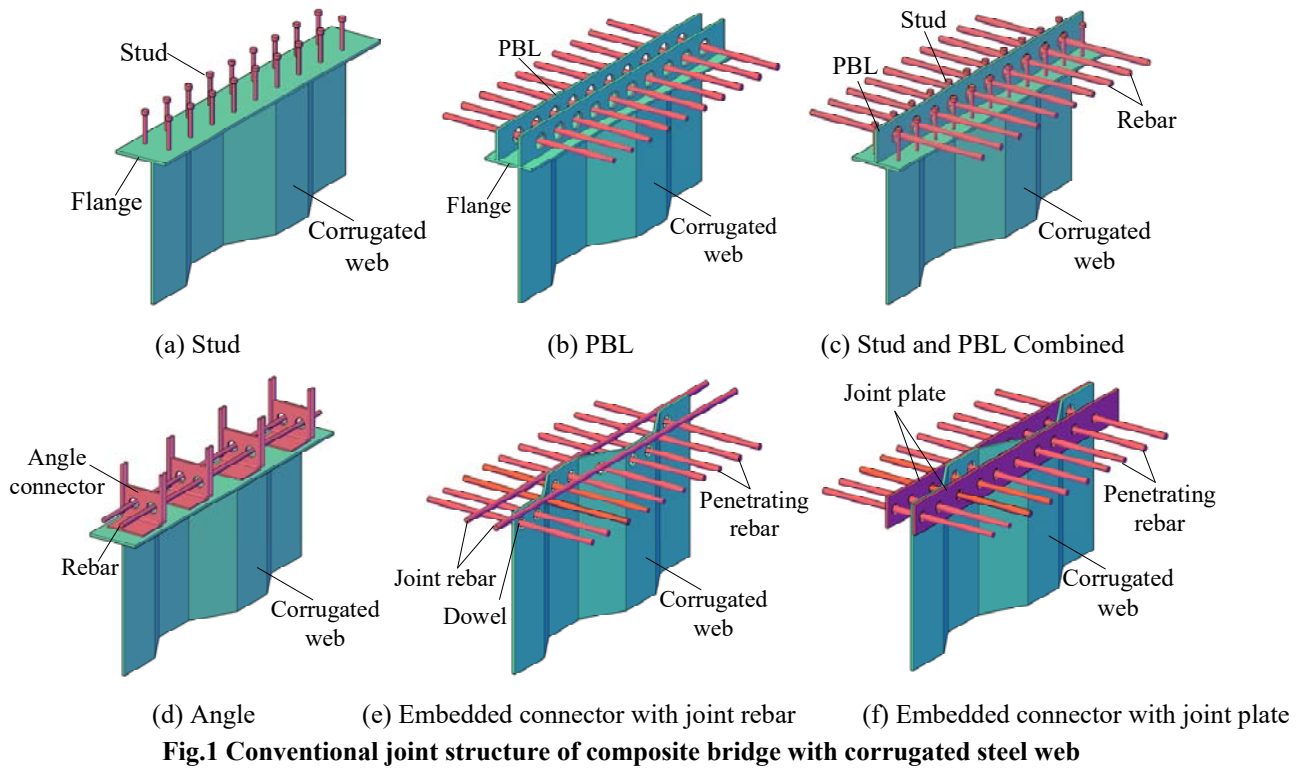
Fig.17 Effect of steel yield strength

Fig.18 Effect of concrete compressive strength

Fig.19 Effect of perforating rebar

Fig.20 Comparison of shear strength from test, FEA and calculation

Figures



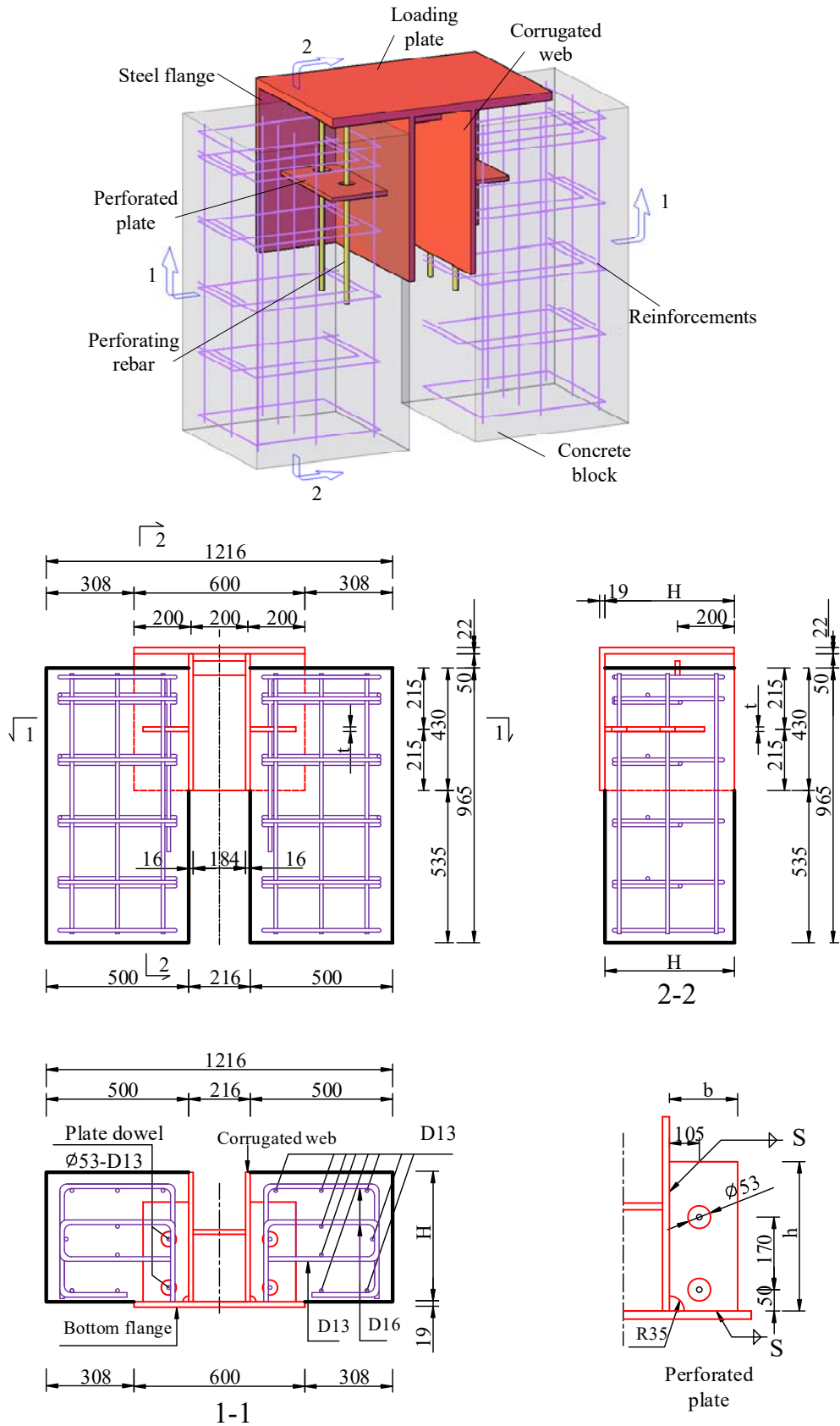


Fig.3 Test specimens /mm

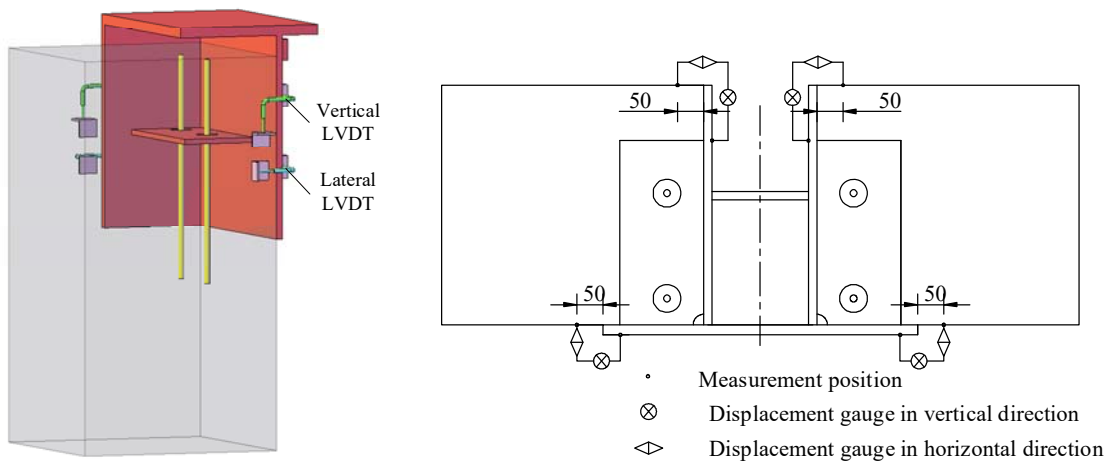


Fig.4 Relative slip measurement /mm

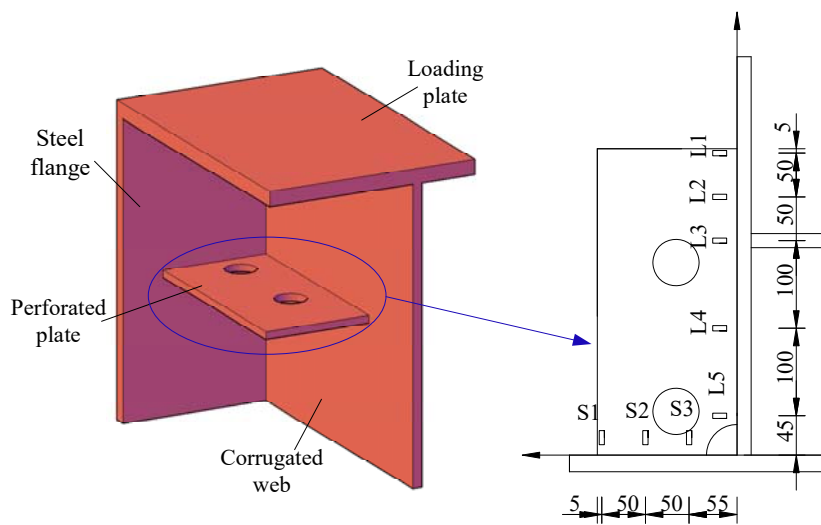
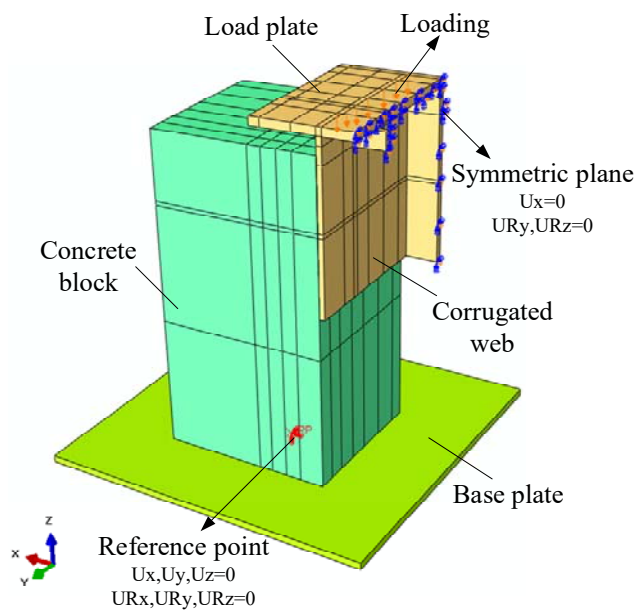


Fig.5 Strain measurement on perforated plate /mm



(a) Full view of the half model

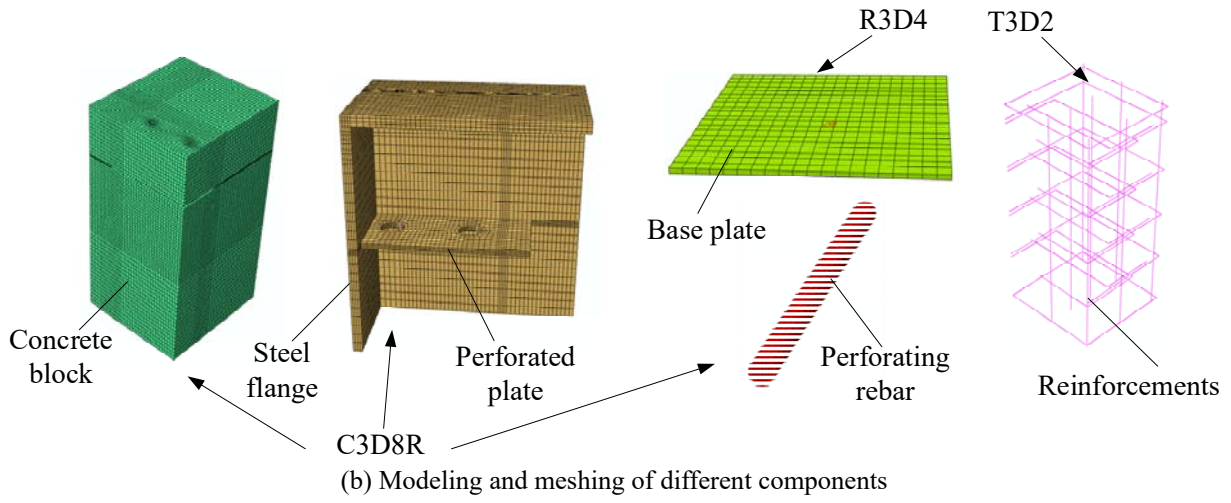
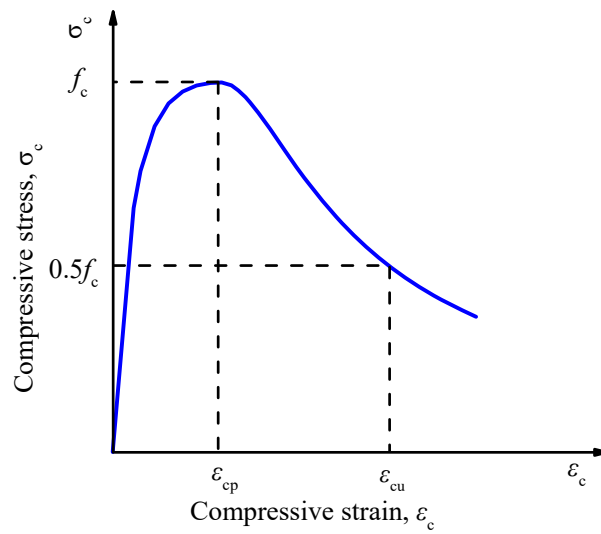
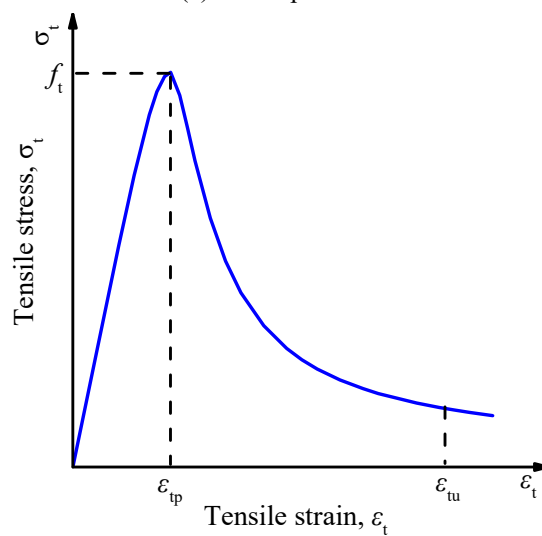


Fig.6 Finite element model of push-out test



(a) In compression



(b) In tension

Fig.7 Material constitution of concrete

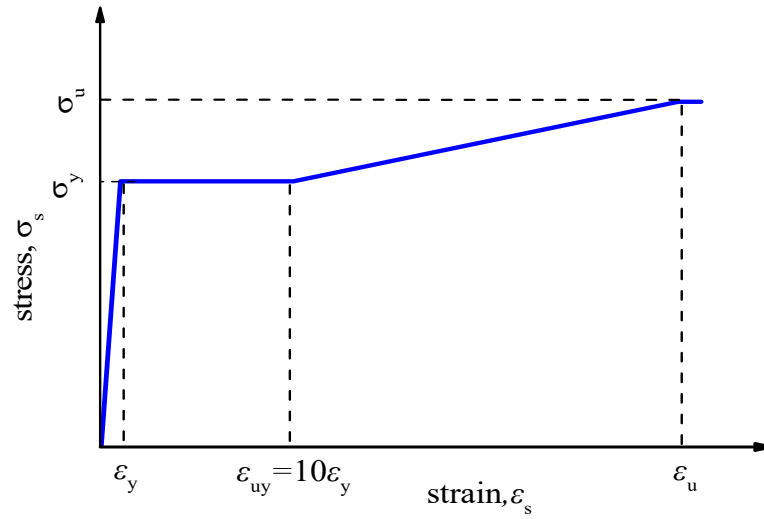


Fig.8 Constitutive law for structural and reinforcement steel

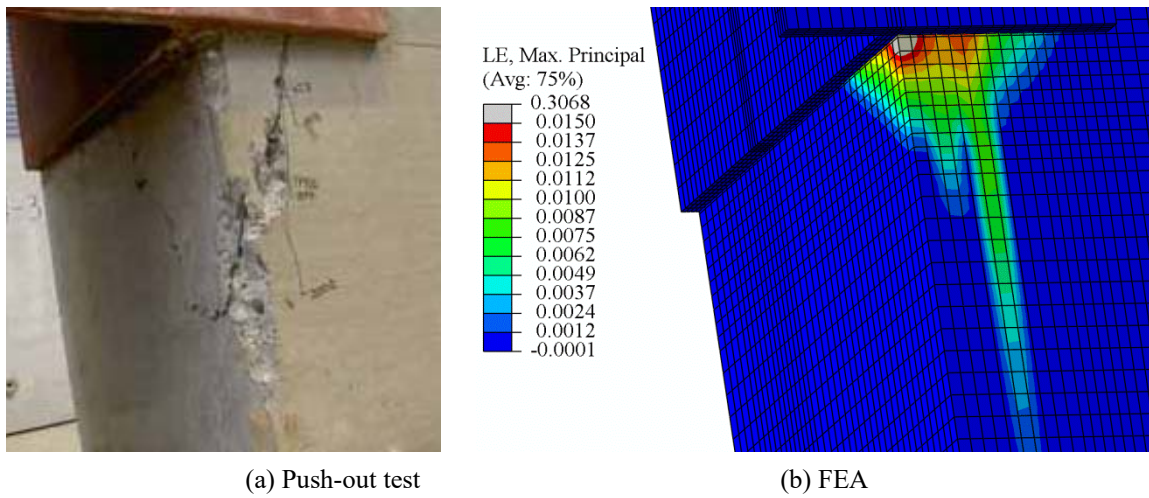


Fig.9 Typical failure mode (SP3)

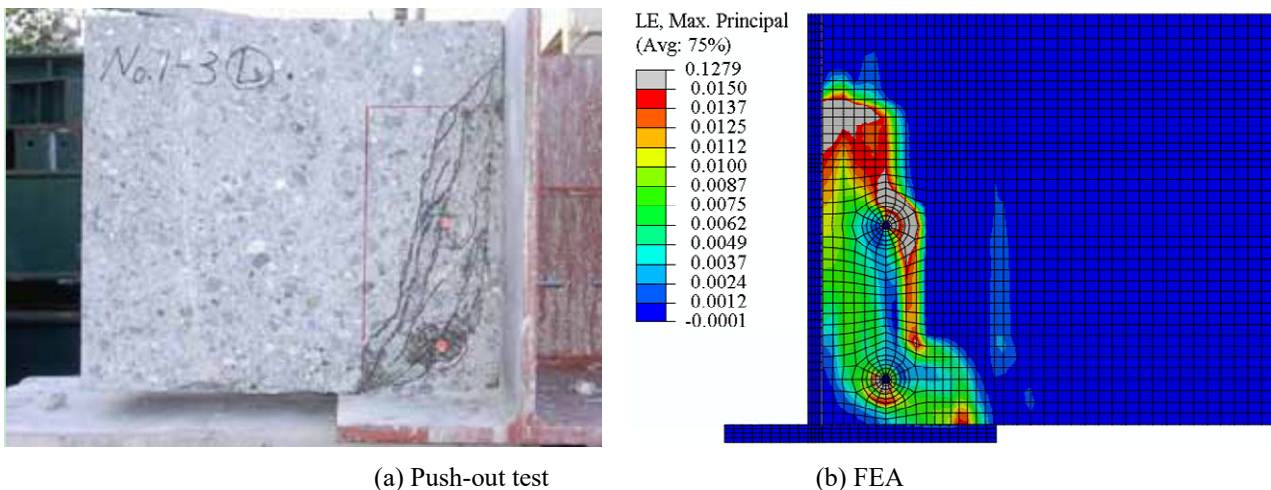
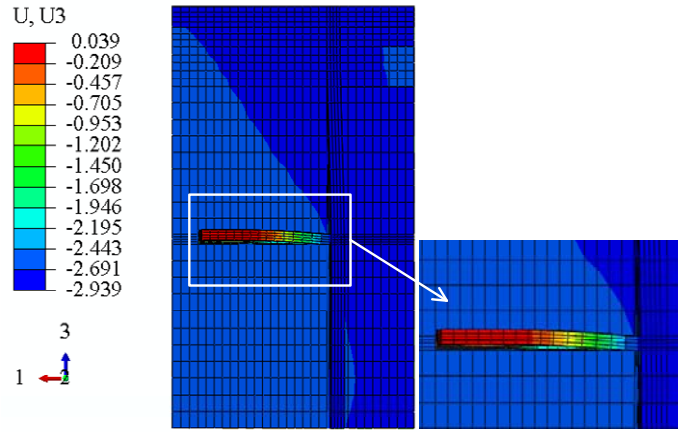


Fig.10 Destructive characteristics on the cutting surface (SP1)

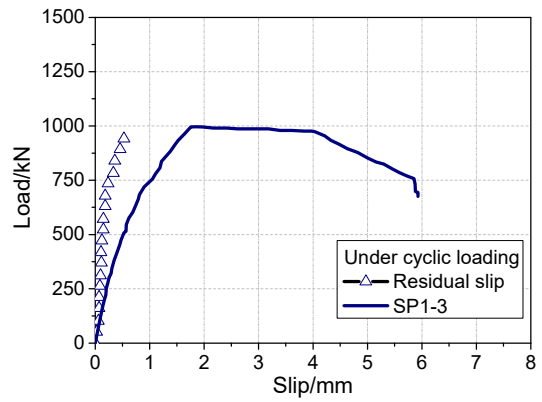
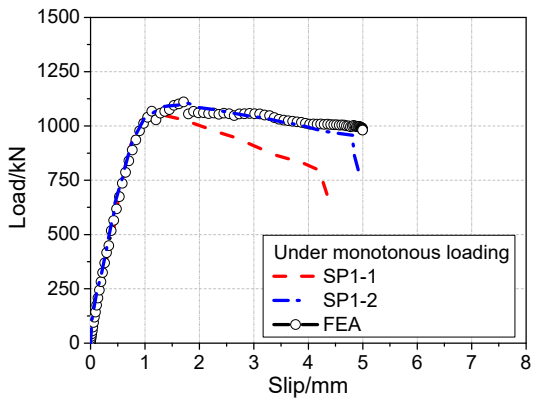


(a) Push-out test

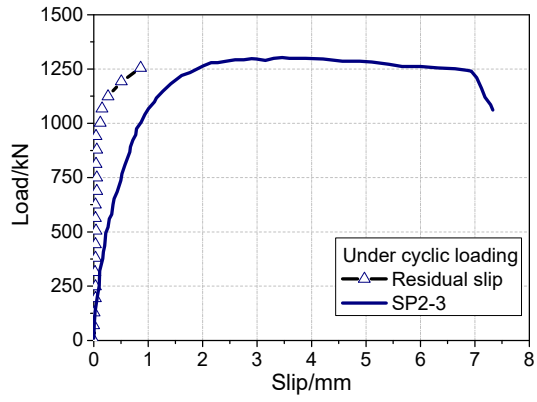
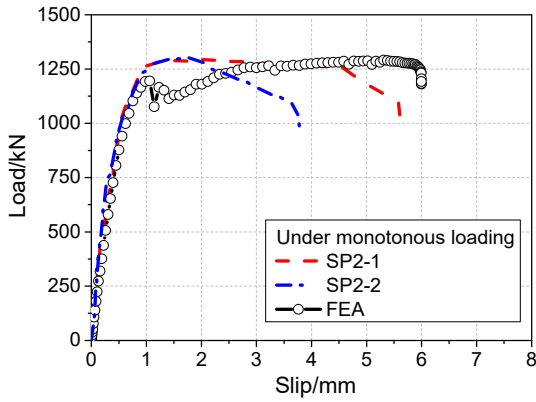


(b) FEA / mm

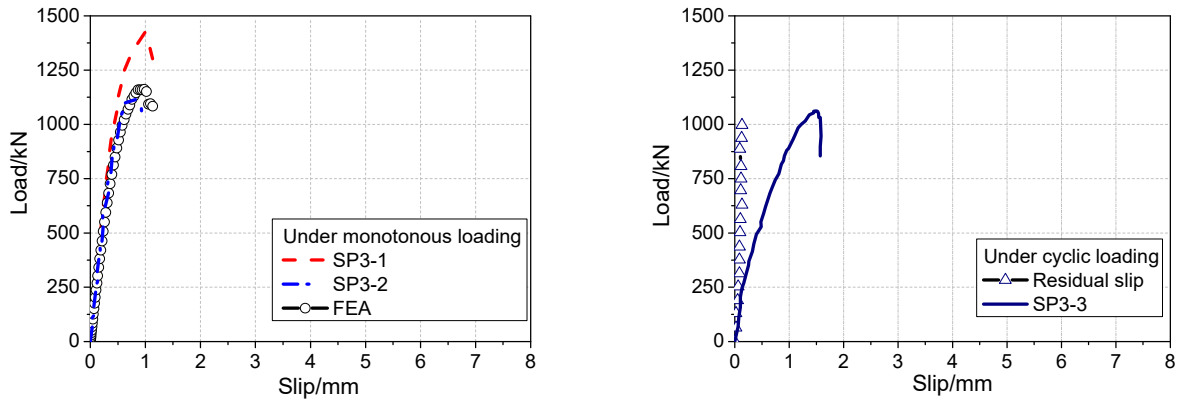
Fig.11 Perforated plate deformation (SP2)



(a) Specimens SP1



(b) Specimens SP2



(c) Specimens SP3

Fig.12 Load-slip curves

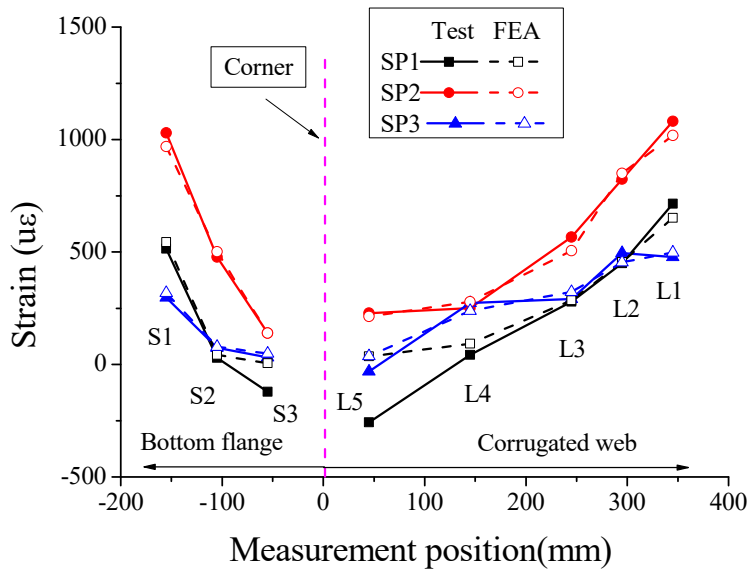
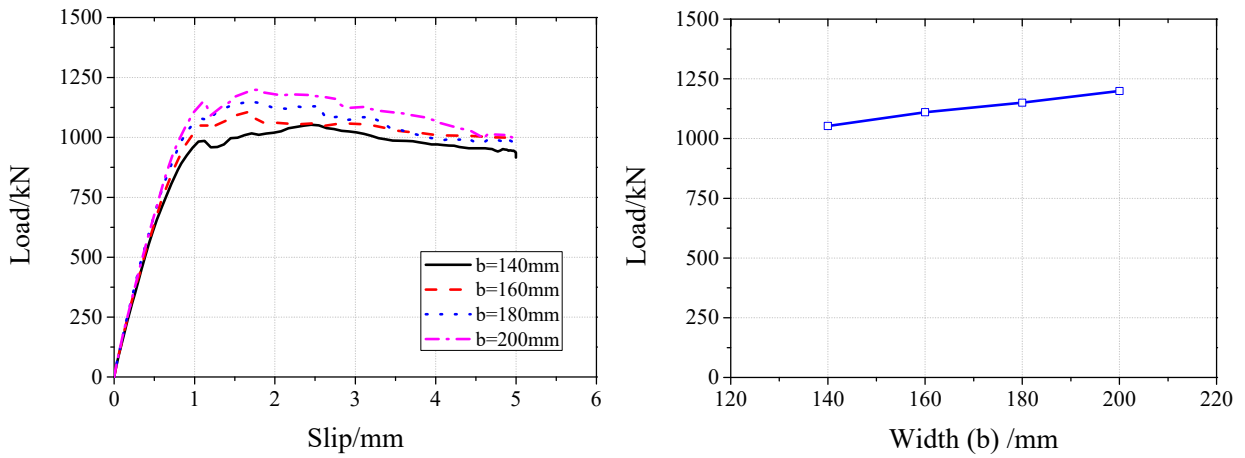


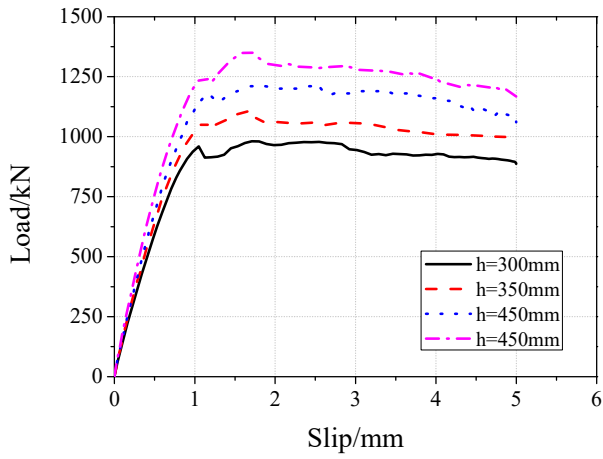
Fig.13 Strain distribution on perforated plate



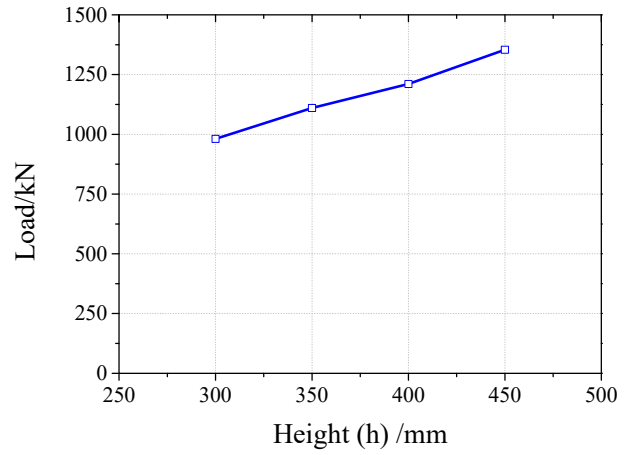
(a) Load-slip curves

(b) Relation between load and perforated plate width b

Fig.14 Effect of perforated plate width

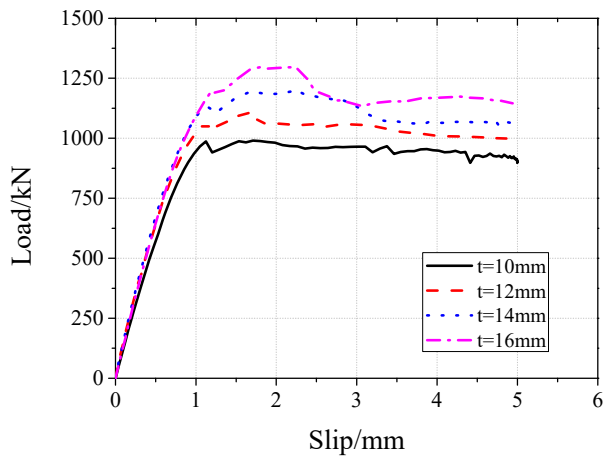


(a) Load-slip curves

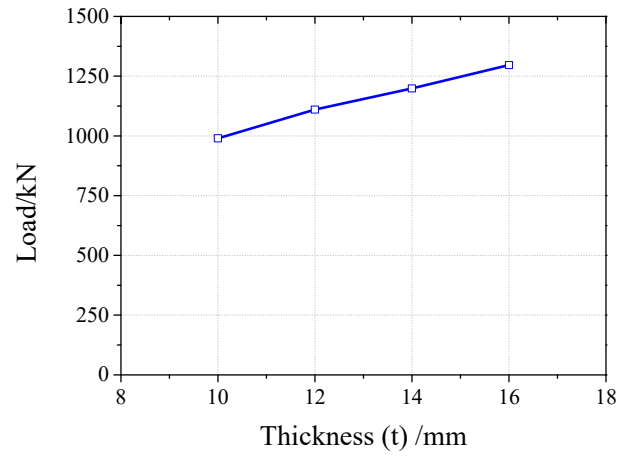


(b) Relation between load and perforated plate height h

Fig.15 Effect of perforated plate height

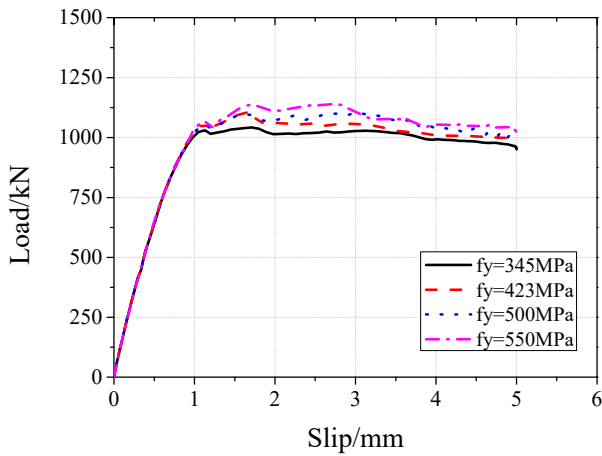


(a) Load-slip curves

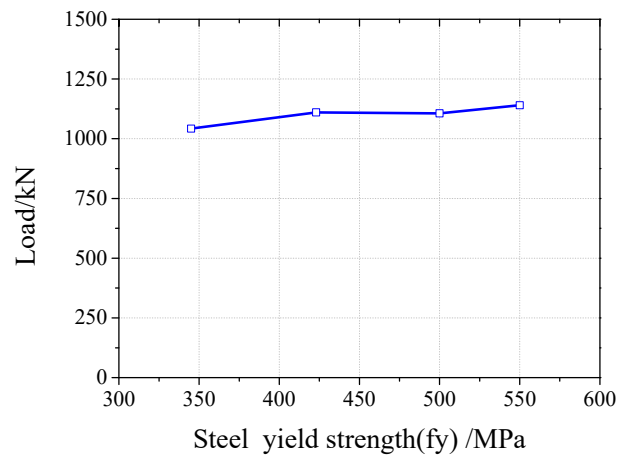


(b) Relation between load and perforated plate thickness t

Fig.16 Effect of perforated plate thickness

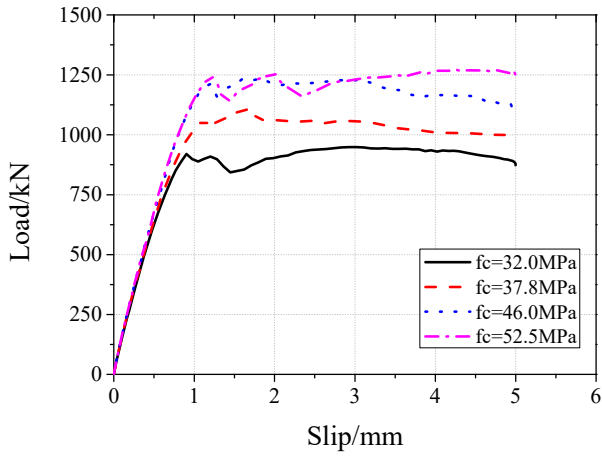


(a) Load-slip curves

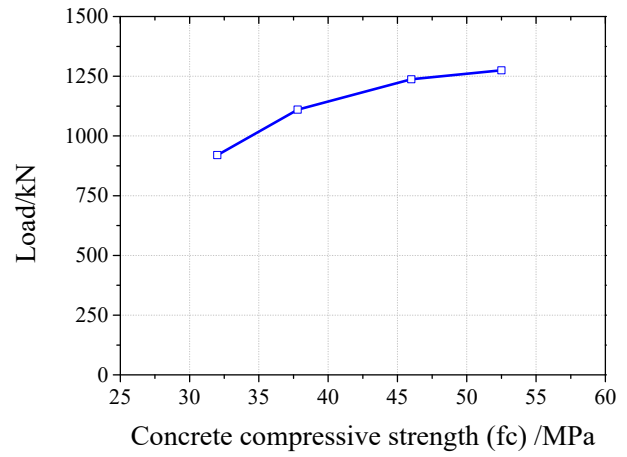


(b) Relation between load and steel yield strength f_y

Fig.17 Effect of steel yield strength

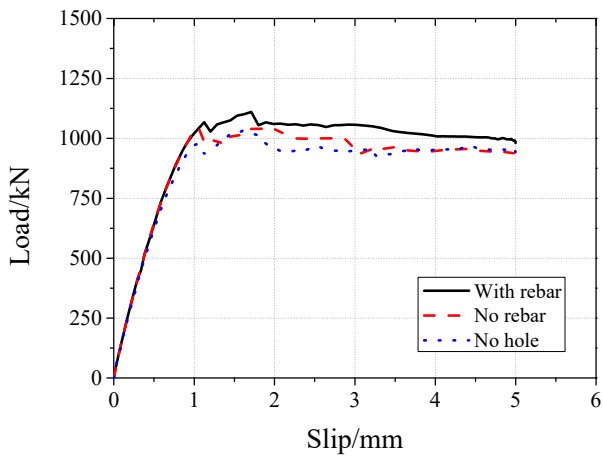


(a) Load-slip curves

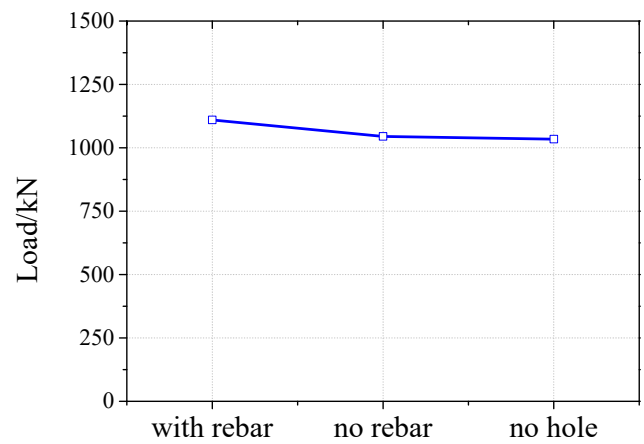


(b) Relation between load and concrete compressive strength f_c

Fig.18 Effect of concrete compressive strength



(a) Load-slip curves



(b) Relation between load and perforating rebar

Fig.19 Effect of perforating rebar

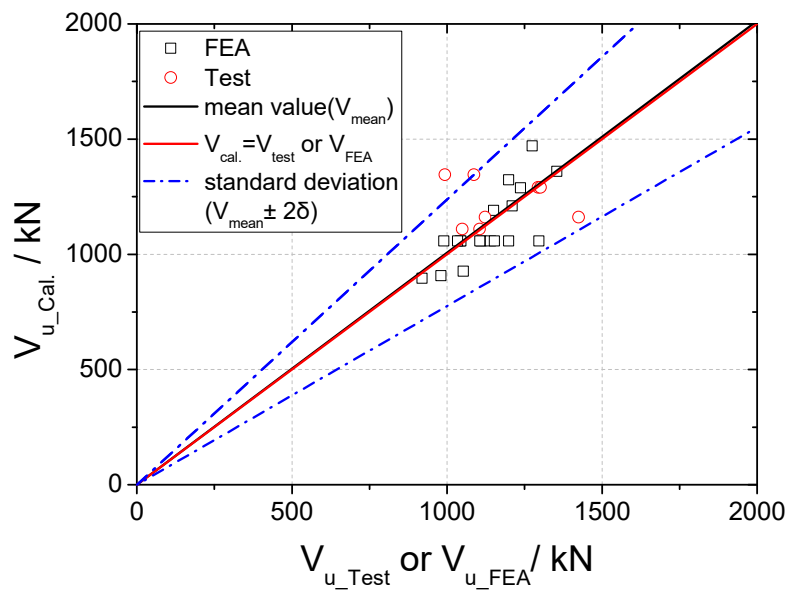


Fig.20 Comparison of shear strength from test, FEA and calculation